WPDTT1-PR(18) 19262

A Mele et al.

Simulation suite for plasma magnetic control at EAST tokamak

Preprint of Paper to be submitted for publication in
Fusion Engineering and Design

This work has been carried out within the framework of the EUROfusion Consortium and has received funding from the Euratom research and training programme 2014-2018 under grant agreement No 633053. The views and opinions expressed herein do not necessarily reflect those of the European Commission.

Simulation suite for plasma magnetic control at EAST tokamak

A. Castaldo[a,b], A. Mele[a,b], R. Albanese[a,b], R. Ambrosino[a,b], G. De Tommasi[a,b], Z. P. Luo[c], A. Pironti[a,b], B. J. Xiao[c], Q. P. Yuan[c]

[a] *Dipartimento di Ingegneria Elettrica e Tecnologie dell'Informazione, Università degli Studi di Napoli Federico II, via Claudio 21, 80125, Napoli, Italy*
[b] *Consorzio CREATE, via Claudio 21, 80125, Napoli, Italy*
[c] *Institute of Plasma Physics, Chinese Academy of Sciences, 350 Shushanhu Rd., 230031, Hefei, Anhui, P.R. China*

Abstract

In view of ITER operations, many experiments are being conducted on the EAST tokamak. In particular, new magnetic control approaches are being developed and need to be tested. In order to design and test a plasma current, position and shape control, an accurate modelling of EAST static equilibria and dynamic plasma evolution is required. Hence, a suite of simulation tools has been developed for the reconstruction of plasma equilibria, the generation of plasma linearized models and for the closed loop testing of magnetic control algorithms. These tools are meant to assess the reliability of such equilibria and models, in order to provide a robust tool for the purposes of control design.

Keywords: Plasma Modeling, Plasma Magnetic Control, EAST, Numerical Simulations

Introduction

A suite of modeling and simulation tools has been developed for the Experimental Advanced Superconducting Tokamak (EAST), with the aim of designing new plasma controllers for standard and alternative configurations, such as double null and snowflake [1].

In the fusion community there exist several codes that allows to perform *physics-oriented* simulations, coupling plasma internal transport with

the Grad-Shafranov magnetic equilibrium (see, for example, JETTO [2], ASTRA [3], CRONOS [4] and JINTRAC [5]). Such codes, due to their complexity and high computational time, cannot be used for control design purposes. It follows that the availability of *engineering-oriented* modeling tools is essential to enable a model-based design of control systems for both plasma magnetic and kinetic control [6, 7, 8, 9, 10, 11]. Despite their simplicity, such engineering-oriented tools permit also to automate the validation and deployment of the plasma control systems. Furthermore, reliable linear models are also used to support design and commissioning of plasma magnetic diagnostic [12], as well as to run inter-shot simulations aimed at optimising the controller parameters.

To achieve the proposed goals with a simple but efficient simulation suite, a trade-off between computational complexity and physical accuracy is needed. Indeed, it is fundamental to catch some aspects of the plasma behavior properly, such as the evolution of the last closed flux surface or the plasma growth rate; the latter, in particular, is strictly linked to the electromagnetic coupling with the passive structures. On the other hand, other phenomena can be neglected, such as, for instance, a detailed description of transport mechanisms.

The simulation suite developed is based on the finite element method (FEM) codes CREATE-NL and CREATE-L [13, 14], which have been exploited to obtain linearized dynamical models of the EAST tokamak. A validation of the linearized models was carried out performing open loop simulations using as inputs experimental signals and comparing the model outputs with experimental data. The results of open loop simulations will be shown in Section 2. Experimental data are stored in a dedicated MDSplus [15] database; for this reason, a set of routines to automatically download these signals has been developed.

Since these tools are specifically designed for plasma control issues, in order to ensure their reliability, the models have then been tested in closed loop reproducing in simulation the experimental control algorithms usually used in EAST pulses and stored in the EAST Plasma Control System (PCS). The closed loop results will be discussed in Sections 3 and 4. The tools have then been applied to develop controller which were tested experimentally: this will be discussed in Section 5

1. Plasma modelling

1.1. Plasma magnetic model description

A tokamak can be seen as a system consisting of the plasma, the passive structures and the active circuits; the 2D FEM code CREATE-NL is designed to solve numerically the Grad-Shafranov equation, which describes the behavior of such a system under the hypothesis of axial symmetry. The output of the code is a static plasma equilibrium. Both CREATE-NL and CREATE-L can be used to obtain a linearized model by means of two different linearization procedures, numerical and analytical in a neighborhood of the equilibrium point, respectively. The general form of a linearized model can be derived starting from the plasma-circuit equation [14]:

$$L\dot{I}(t) + RI(t) = u(t) - L_E\dot{w}(t)\,, \tag{1}$$

where:

- L is the mutual inductance matrix among the active coils, the passive structures and the plasma;
- R is the resistance matrix;
- L_E is the disturbances matrix used to take into account possible profile variations;
- $I(t) = [I_a(t)^T\ I_p(t)^T\ I_{pl}(t)]^T$ is currents vector which includes currents on active circuits, eddy currents and plasma current respectively;
- $u(t) = [U_{PF}(t)\ U_{IC}(t)]^T$ is the input vector composed by voltages on Poloidal Field Coils (PFCs in the following) and Internal Coils (IC in the following) circuit;
- $w(t) = [\beta_p(t)\ l_i(t)]^T$ is the disturbances vector where β_p and l_i are measures of the plasma internal distributions of pressure and current, respectively;

From plasma-circuit model (1) choosing as state variables $x(t) = I(t)$ we obtain:

$$\dot{x}(t) = Ax(t) + Bu(t) + E\dot{w}(t) \tag{2a}$$

$$y(t) = Cx(t) + Du(t) + Fw(t)\,, \tag{2b}$$

where:

- $A = -L^{-1}R;\ B = L^{-1};\ E = -L^{-1}L_E;$
- $y(t)$ is the output vector,including plasma current, position and flux of both plasma centroid and active X-point, fluxes corresponding to active control segments, magnetic field and flux measurements;

1.2. Hybrid driven Poloidal Field Coils

The linear model presented in (2a) and (2b) is the standard output of CREATE-L code. In this model it is assumed that all the coils $I(t)$ are voltage driven. However, the vertical stabilization system adopted in the EAST PCS exploits the in-vessel circuits in current-driven mode. Furthermore, the experimental current signals resulted to be more reliable than the measured voltages on active circuits. For these reasons, a change of variable was needed in order to have a subset of coils in current driven mode.

First of all let us consider the plasma-circuit equation (1). The current vector can be split as:

$$I(t) = [I_{VD}^T\ I_{CD}^T]^T\,, \tag{3}$$

where I_{VD} and I_{CD} indicate the currents in the voltage driven and current driven circuits respectively. The voltage driven circuits also include the plasma and the passive elements where $U = 0$. Plasma-circuit equation can be then rewritten as:

$$\begin{bmatrix} L_{11} & L_{12} \\ L_{21} & L_{22} \end{bmatrix} \begin{bmatrix} \dot{I}_{VD} \\ \dot{I}_{CD} \end{bmatrix} = - \begin{bmatrix} R_{11} & 0 \\ 0 & R_{22} \end{bmatrix} \begin{bmatrix} I_{VD} \\ I_{CD} \end{bmatrix} + \begin{bmatrix} U_{VD} \\ U_{CD} \end{bmatrix}\,. \tag{4}$$

For the sake of simplicity, the disturbances have been neglected; the reader can easily include them in the input vector applying simple matrix algebra to the equations (2a), (2b). Experimental traces of β_p and l_i reconstructed during EAST experiments are available in EFIT database [16]. Let now introduce the magnetic fluxes defined as $\Psi = LI$, as new state variables. Since I_{CD} will be the new input vector, Ψ can be written as:

$$\Psi = L_{11}I_{VD} + L_{12}I_{CD} \Rightarrow I_{VD} = L_{11}^{-1}\Psi - L_{11}^{-1}L_{12}I_{CD}\,. \tag{5}$$

Substituting (5) in (4) we get:

$$\dot{\Psi} = -R_{11}L_{11}^{-1}\Psi + R_{11}L_{11}^{-1}L_{12}I_{CD} + U_{VD} \Rightarrow \dot{\Psi} = A\Psi + B\begin{bmatrix} U_{VD} \\ I_{CD} \end{bmatrix}, \qquad (6)$$

where:

- $A = -R_{11}L_{11}^{-1}$;
- $B = \begin{bmatrix} I & R_{11}L_{11}^{-1}L_{12} \end{bmatrix}$ where I is the identity matrix;

For the output equation, substituting (5) in (2b) we get:

$$y(t) = C_1 I_{VD} + C_2 I_{CD} + D_1 U_{VD} \Rightarrow y(t) = C\Psi + D\begin{bmatrix} U_{VD} \\ I_{CD} \end{bmatrix}, \qquad (7)$$

where:

- $C = C_1 L_{11}^{-1}$;
- $D = \begin{bmatrix} D_1 & C_2 - C_1 L_{11}^{-1} L_{12} \end{bmatrix}$.

In order to have a good estimation of plasma current behavior in the time simulation interval, an equivalent plasma resistance can be obtained by means of experimental flux measurements and making use of Faraday-Newman's law. Once computed equivalent plasma resistance, it's possible to apply to the plasma circuit an equivalent voltage in order to take into account also possible current drive effects.

1.3. Main controlled outputs for the shape control system

EAST control system implements two different control logics for the shape control, namely RZIP and Isoflux (for a detailed discussion, see paragraph 3). In particular, the Isoflux control logic aims at taking to zero the poloidal flux differences between the active X-point and some specific points, defined as the intersections between some control segments and the desired plasma boundary. For this reason, a good reconstruction of the fluxes on these segments is essential. To achieve this purpose, a set of 10 virtual flux sensors has been placed on each of the segments available for shape control as shown in Fig. 1; the flux in the actual control points (whose positions can be retrieved from the EFIT dedicated database) is then obtained interpolating.

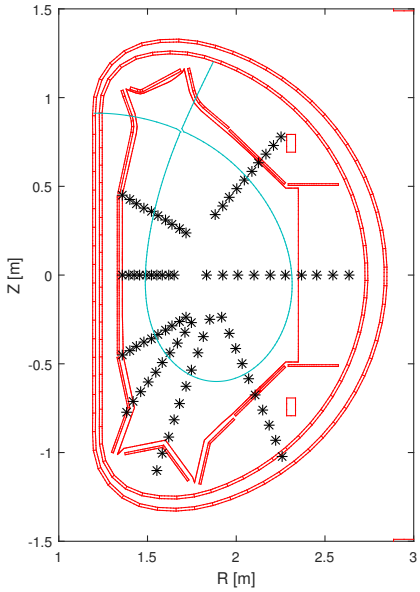

Figure 1: Virtual flux sensors placed on the control segments for upper single null pulse #75008. In blue is reported plasma boundary reconstructed using EFIT database.

In section 2, the comparisons between experimental and simulated fluxes in some of the control points will be presented.

The Isoflux control logic includes also a direct control of the position of the null-points, either only the active one or both active and non active, depending on the configuration. Furthermore, the knowledge of the flux at the X-point is necessary for the shape control. For these reasons, a procedure for an accurate identification of the X-points dynamics in terms of radial and vertical position and poloidal flux has been implemented. The starting assumption is that the X-point is a stationary point for the poloidal flux. Hence, a quadratic function to estimate the flux in a desired region of the poloidal plane containing the X-point has been considered:

$$\Psi(r,z) = a^2 r + brz + cz^2 + dr + ez + f\,. \tag{8}$$

To determine the vector coefficients $[a\ b\ \cdots\ f]^T$, two grids of $n \times n$ virtual flux sensors surrounding the expected X-point positions have been considered.The measurements of the virtual flux sensors are derived by a reconstructed flux map. Since the magnetic fluxes in the points of the grids are known, the vector coefficients can be calculated as:

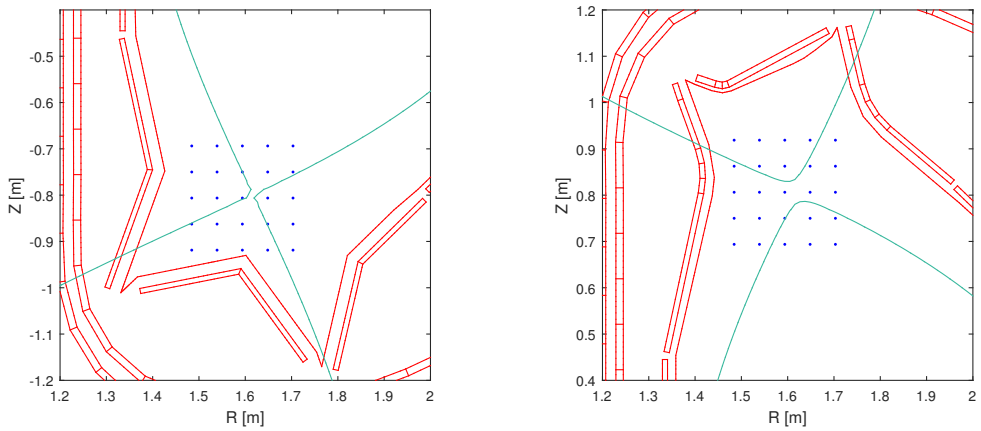

Figure 2: Box of virtual flux sensors used to estimate position and flux of lower X-point (left) and upper X-point (right). The reconstruction of plasma boundary for DN pulse #46530 at 3 s from EFIT database is reported in blue color.

$$\begin{bmatrix} r_1^2 & r_1 z_1 & z_1^2 & r_1 & z_1 & 1 \\ r_2^2 & r_2 z_2 & z_2^2 & r_2 & z_2 & 1 \\ \dots & \dots & \dots & \dots & \dots & \dots \\ r_n^2 & r_n z_n & z_n^2 & r_n & z_n & 1 \end{bmatrix} \begin{bmatrix} a \\ b \\ c \\ d \\ e \\ f \end{bmatrix} = \begin{bmatrix} \Psi(r_1, z_1) \\ \Psi(r_2, z_2) \\ \dots \\ \Psi(r_n, z_n) \end{bmatrix} \Rightarrow$$
$$\Rightarrow \begin{bmatrix} a \\ b \\ c \\ d \\ e \\ f \end{bmatrix} = \begin{bmatrix} r_1^2 & r_1 z_1 & z_1^2 & r_1 & z_1 & 1 \\ r_2^2 & r_2 z_2 & z_2^2 & r_2 & z_2 & 1 \\ \dots & \dots & \dots & \dots & \dots & \dots \\ r_n^2 & r_n z_n & z_n^2 & r_n & z_n & 1 \end{bmatrix}^{\dagger} \begin{bmatrix} \Psi(r_1, z_1) \\ \Psi(r_2, z_2) \\ \dots \\ \Psi(r_n, z_n) \end{bmatrix}, \tag{9}$$

where $[\cdot]^{\dagger}$ denotes the Moore-Penrose pseudoinverse matrix. Once the vector coefficients are computed, position and flux of X-point can be evaluated. Since X-points are stationary points, it is:

$$\vec{\nabla}\Psi(r_{xp}, z_{xp}) = \left.\frac{\partial \Psi}{\partial r}\right|_{\substack{r=r_{xp} \\ z=z_{xp}}} \hat{r} + \left.\frac{\partial \Psi}{\partial z}\right|_{\substack{r=r_{xp} \\ z=z_{xp}}} \hat{z} = 0\,, \tag{10}$$

where r_{xp} and z_{xp} indicate radial and vertical position of X-point respectively. Computing the magnetic flux gradient in (r_{xp}, z_{xp}) we have:

$$\begin{bmatrix} 2a & b \\ b & 2c \end{bmatrix} \begin{bmatrix} r_{xp} \\ z_{xp} \end{bmatrix} + \begin{bmatrix} d \\ e \end{bmatrix} = \begin{bmatrix} 0 \\ 0 \end{bmatrix} \Rightarrow \begin{bmatrix} r_{xp} \\ z_{xp} \end{bmatrix} = - \begin{bmatrix} 2a & b \\ b & 2c \end{bmatrix}^{-1} \begin{bmatrix} d \\ e \end{bmatrix}. \tag{11}$$

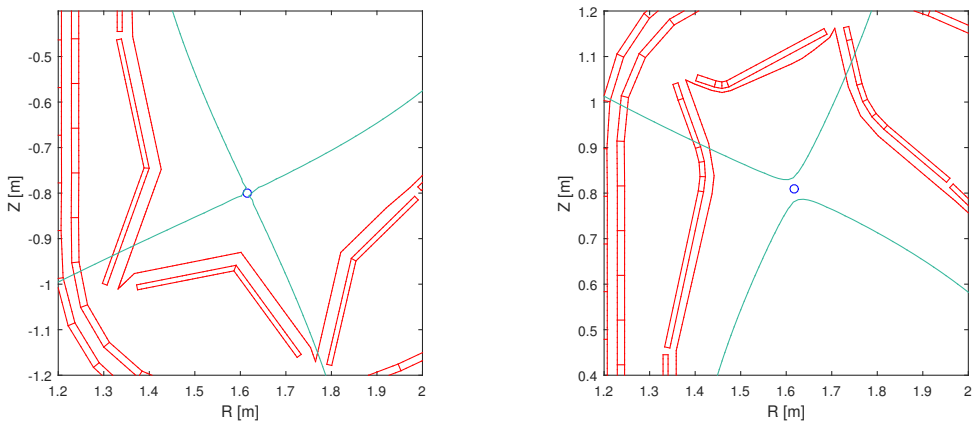

Figure 3: Static identification of active (left figure) and non active (right figure) X-point for for DN pulse #46530. In blue is reported plasma boundary reconstructed using EFIT database.

Finally, the X-point flux can be computed by means of equation (8). In Fig. 3 are shown the results of the procedure applied to DN pulse #46530. Indeed, in this case, starting from the EFIT flux map reconstruction, a $n \times n$ grid of virtual sensor with $n = 5$ and a distance of around 5 cm between two adjacent sensors has been considered, as shown in Fig. 2 The error between EFIT reconstruction (blue solid line) and the estimation (blue circle) is less than 1 mm for both the active and non-active X-points, hence proving the goodness of the method.

It is worth to mention that the proposed method can be applied to divertor configurations without close null points. In case of alternative configurations with close null points, such as snowflake, a quadratic expansion is not sufficient to properly fit the flux map in the vicinity of the null points and alternative solutions might entail a higher order polynomial fitting or a numerical estimate of the poloidal flux gradient over a finer grid.

2. Open loop validation

In this section, comparisons between experimental and open loop simulated data in terms of plasma current, radial and vertical position of plasma centroid, radial and vertical position and flux of both active and non active X-point, magnetic field and flux measurements and fluxes on control segments will be presented. Since elongated plasmas are vertically unstable, a procedure to simulate backward in time the unstable eigenvalue has been employed (more references can be found in [17]) using as inputs the currents on active circuits, an equivalent plasma voltage and the profile parameters poloidal beta and internal inductance (treated as disturbances). Figs. 4- 9 report the results of the comparisons. The good matching between simulated and experimental data prove the accuracy of the linearized models generated.

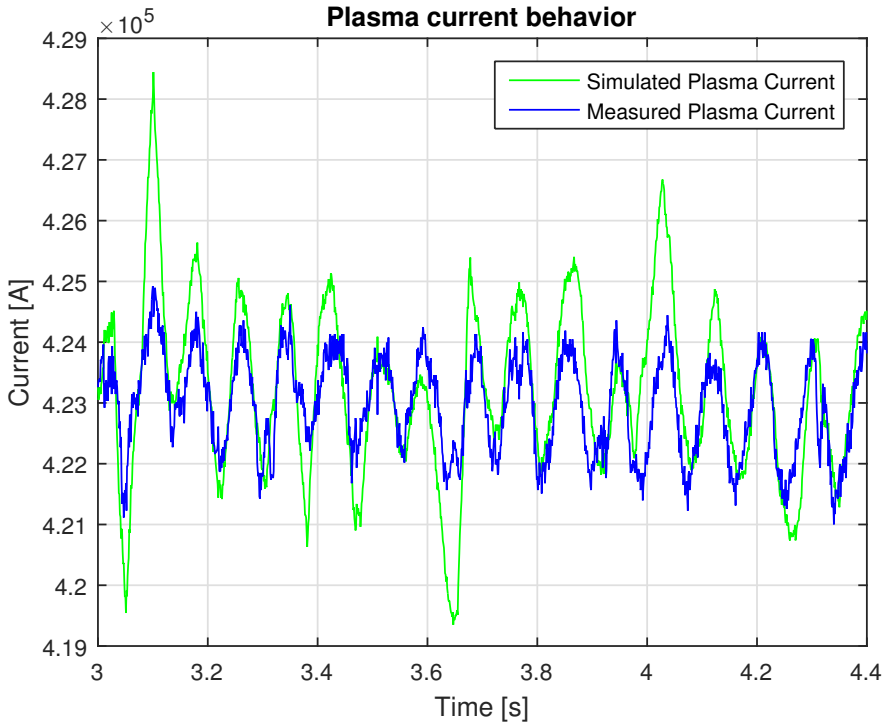

Figure 4: Comparison between simulated plasma current (green solid line) and experimental plasma current (blue solid line) for pulse #69449.

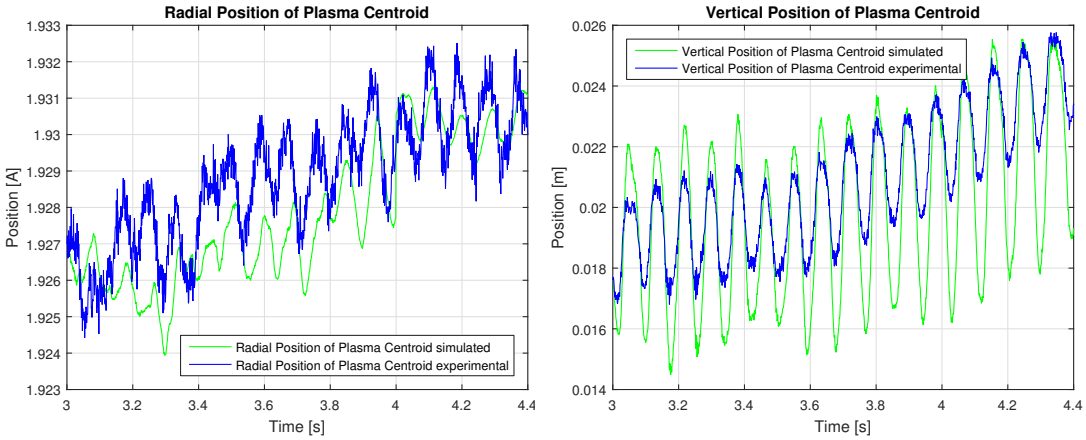

Figure 5: Comparison between simulated (green solid line) and experimental (blue solid line) plasma centroid radial (left figure) and vertical (right figure) position for pulse #69449.

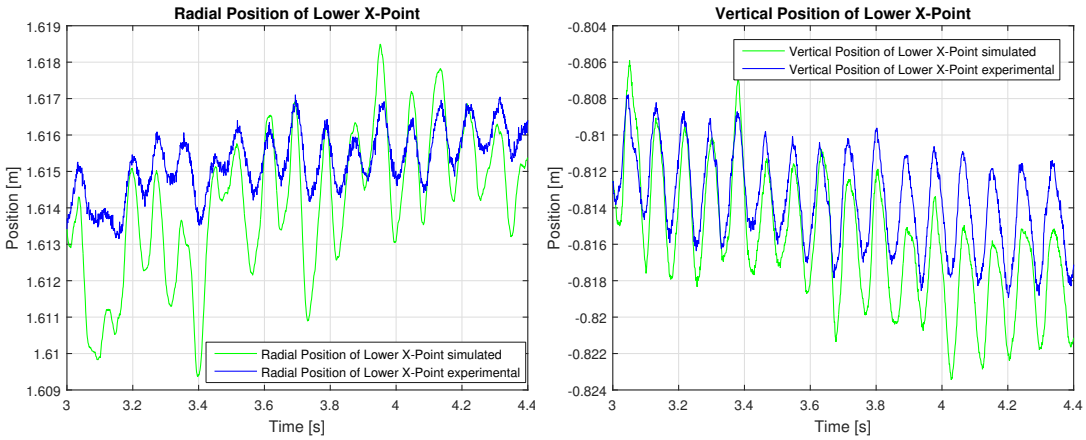

Figure 6: Comparison between simulated (green solid line) and experimental (blue solid line) plasma Lower X-point radial (left figure) and vertical (right figure) position for pulse #69449.

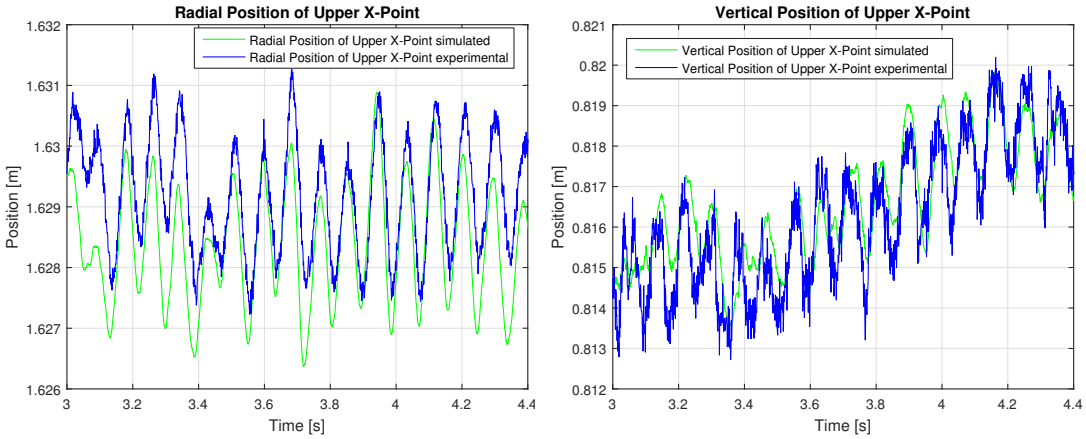

Figure 7: Comparison between simulated (green solid line) and experimental (blue solid line) plasma Upper X-point radial (left figure) and vertical (right figure) position for pulse #69449.

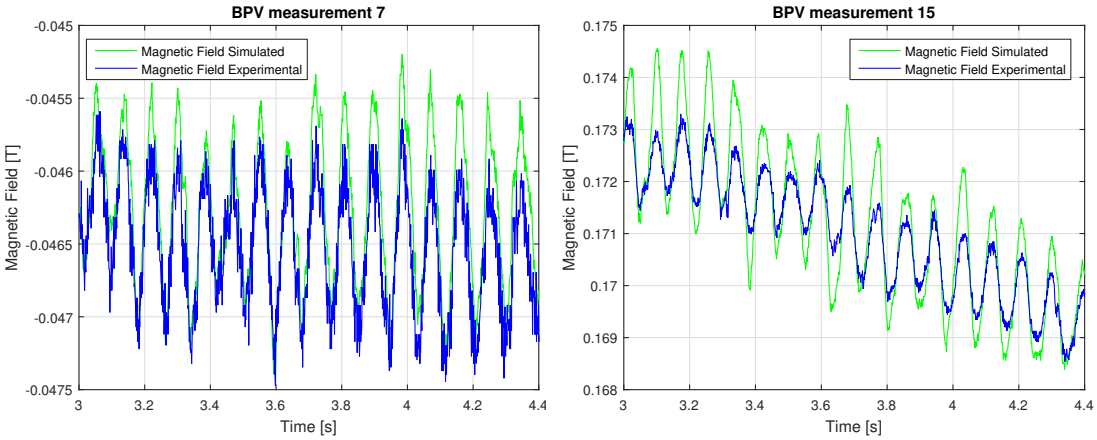

Figure 8: Comparison between simulated (green solid line) and experimental (blue solid line) magnetic measurements BPV 7 (left figure) and BPV 15 (right figure) for pulse #69449.

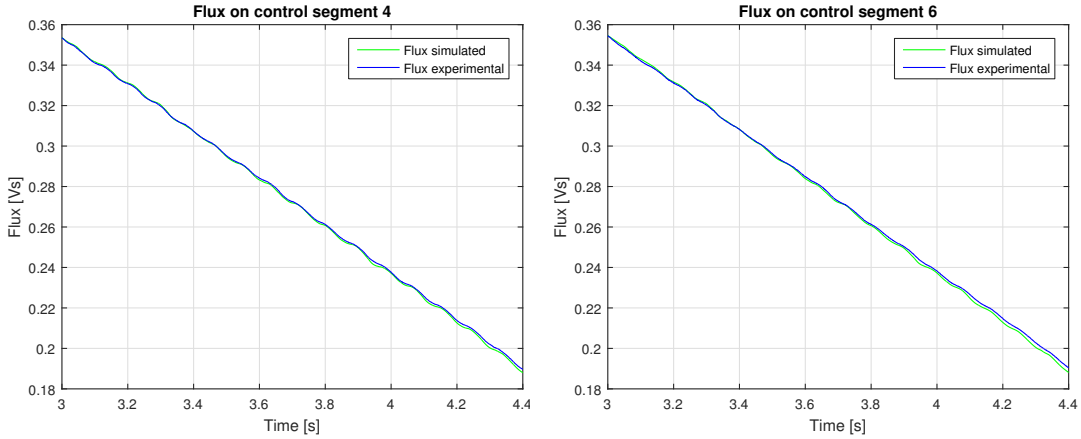

Figure 9: Comparison between simulated (green solid line) and experimental (blue solid line) magnetic flux for control segment 4 (left figure) and 6 (right figure) for pulse #69449.

3. Modelling of the EAST Magnetic Control System

Since the final aim of the models described in the previous section is the design of new control algorithms for the EAST plasma, it is necessary to assess their reliability in closed loop. In order to carry out this task, it is then fundamental to reproduce correctly the EAST PCS control algorithms. In particular, the two main control logics adopted at EAST are:

- **RZIP**: in this operation mode, the controlled quantities are the plasma current (I_p) and the radial and vertical position of the plasma centroid (R, Z).
- **Isoflux**: this operation mode aims at controlling the plasma shape by regulating to zero the difference between the flux at the null-point and the flux at some target positions; the fluxes are estimated by means of a real-time reconstruction code (RT-EFIT [18] or PEFIT [19]). In addition, the plasma current and the null-point position are controlled to a desired value; alternatively, instead of controlling the X-point position, the magnetic field in that point can be regulated to zero. For double-null plasmas, also the position of the 2^{nd} null and the distance between the isoflux surfaces passing through the two nulls (dr_{sep}) are controlled. For the purposes of this discussion, we will focus on single null plasmas.

Both control logics generate references for the inner PFC current control loop. Furthermore, in both cases a vertical stabilizing controller is needed. At EAST, this controller usually actuates the IC coils in current driven mode. The architecture of the PCS is shown in Fig. 10. For more details, the interested reader is referred to [20].

As it can be seen in Fig. 10, most of the controllers employed in the EAST PCS contain proportial-integral-derivative (PID) regulators. The standard PID used at EAST is equipped with an input low pass filter, i.e.:

$$U(s) = \frac{1}{1+sT_p} \cdot \left(K_p + K_i \frac{1}{1+sT_i} + K_d \frac{sT_d}{1+sT_d} \right) \cdot E(s)\,, \qquad (12)$$

where $U(s)$ and $E(s)$ denote the control output and the input error respectively.

The parameters for each of the controllers are stored on the EAST PCS dedicated server, and can be made accessible via MDSplus. Knowing these

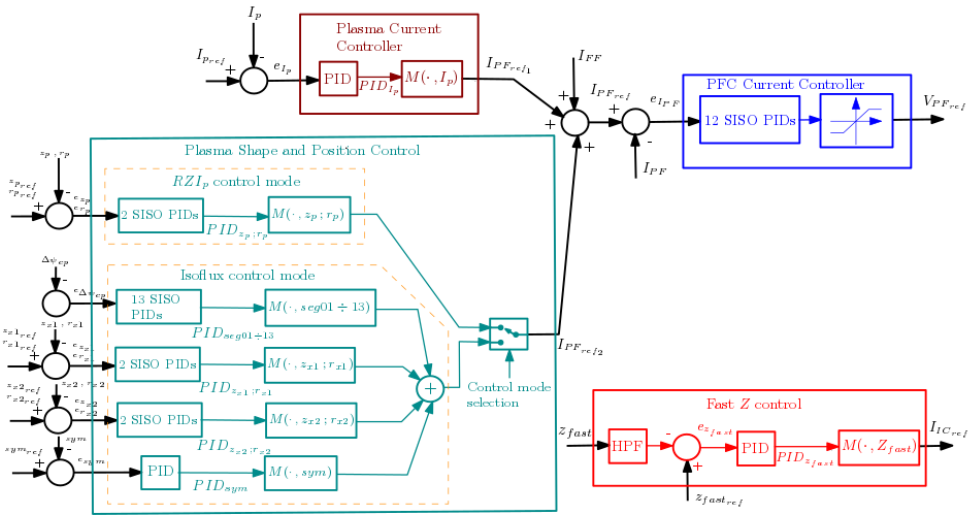

Figure 10: Architecture of the EAST PCS.

parameters, all the controllers can be tested in open loop, feeding in the experimental errors and comparing the simulated outputs with the real ones. An example is shown in Fig. 11 for pulse #74104.

Each of the controller's outputs is post-multiplied by a column vector which distributes opportunely the control action to the PFCs; these vectors are all collected in a single matrix, called *M matrix* in the PCS jargon, as it can be seen from Fig. 10. Each row of the M-matrix corresponds to one circuit: by summing the plasma current, position and/or shape controllers outputs weighted by the M-matrix elements and suitable feedforwards, the current references for the PF Current controller are obtained.

On the other hand, the vertical stabilization loop (called "Fast Z" controller) is separated from the other ones, and relies on a couple of in-vessel coils, connected in anti-series. This loop takes as a feedback a linear combination of magnetic sensors placed along the chamber walls, which is then derived by means of a derivative filter in the form

$$Y_d(s) = \frac{sT_f}{1+sT_f} \cdot Y(s)\,. \tag{13}$$

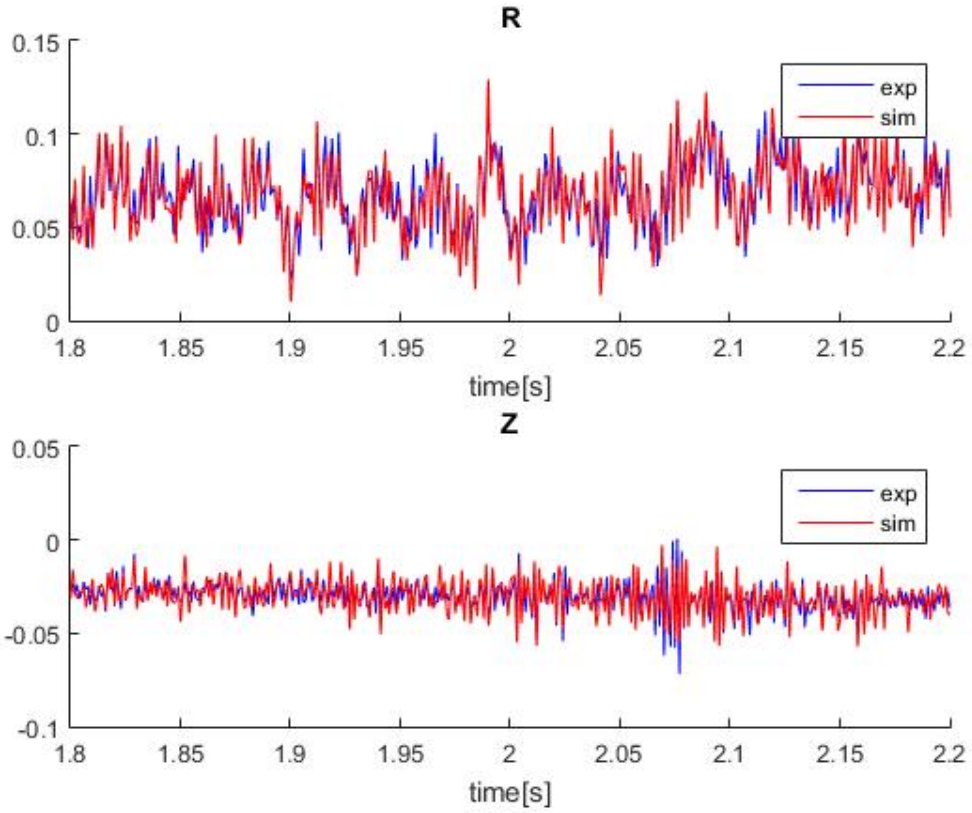

Figure 11: Plasma centroid position controller output for pulse #74104. The small discrepancies are due to a sub-sampling of the experimental error signal.

Usually, the time constant T_f is kept fixed to 0.1 s. The controller output is the current reference for the IC circuit; when the *Fast Z* controller is active, these coils are usually operated in current-driven mode.

4. Closed loop validation

Once the reliability of both the plasma linearized model and the control system algorithms has been assessed, actual EAST experiments can be reproduced by means of closed loop simulations.

The pulse is simulated using the experimental control parameters, references and disturbances. In particular, since the disturbances definition

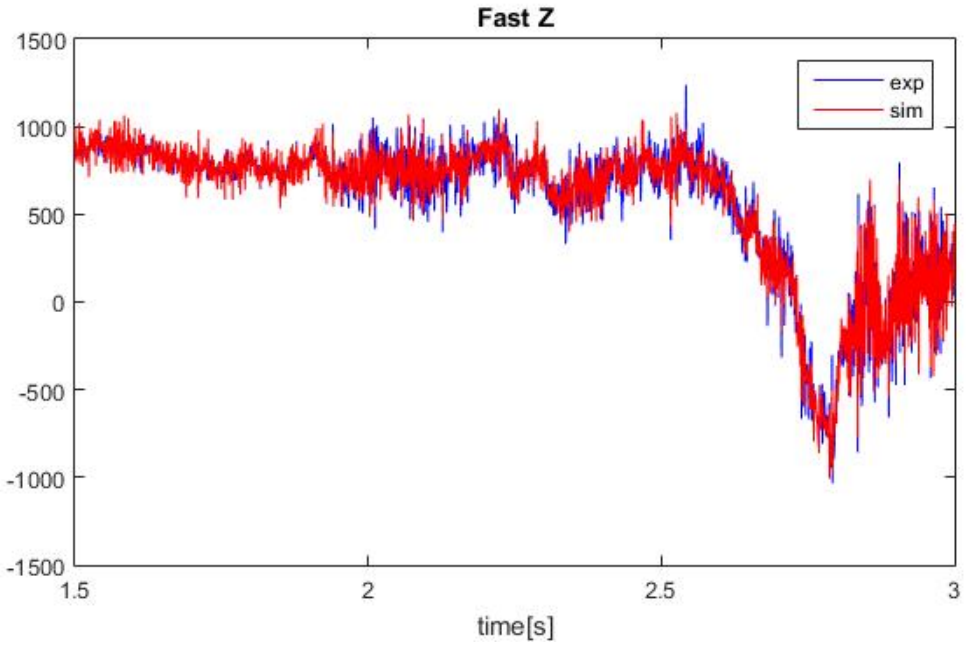

Figure 12: Fast Z controller (including the high pass filter) output for pulse #74104. The small discrepancies are due to a subsampling of the experimental feedback signal.

between EFIT and the CREATE codes is different, some preliminary operations need to be done. These definitions are

$$\beta_{p,CREATE} = \frac{W_p}{W_m}\,, \tag{14}$$

$$\beta_{p,EFIT} = \frac{4W_p}{\mu_0 R_{ref} I_p^2}\,, \tag{15}$$

$$l_{i,CREATE} = \frac{4W_m}{\mu_0 R_0 I_p^2}\,, \tag{16}$$

$$l_{i,EFIT} = \frac{4W_m}{\mu_0 R_{ref} I_p^2}\,, \tag{17}$$

where W_p is the average kinetic pressure, W_m is the average magnetic pressure, R_0 is the plasma major radius and R_{ref} is defined as

$$R_{ref} = \frac{2V_p}{l_p^2}\,, \tag{18}$$

where V_p is the plasma volume and l_p is the plasma perimeter; $R - ref$ approaches R_0 in the large aspect ratio approximation.

As it can be seen from equations 14-17, the value of poloidal beta adopted by CREATE-L is related to the EFIT definition via the following relation

$$\beta_p = \frac{\beta_{p,EFIT}}{l_{i,EFIT}}\,. \tag{19}$$

The definition of the internal inductance adopted by EFIT, instead, is different from the one adopted by CREATE-L because it includes some geometrical factors related to the plasma shape. In the hypothesis that the plasma shape is almost constant during the flat top phase, a good approximation is

$$l_i = l_{i,EFIT} \cdot k\,, \tag{20}$$

where the constant k must be determined opportunely.

Furthermore, a grid of 30×30 virtual flux sensors covering all the vacuum chamber has been used in order to reconstruct the flux map and some quantities of interest (i.e. by means of the procedures described in sec. 1.3 for what concerns the position of the null points, using a subset of the whole grid chosen in the surroundings of the reference position of the X-point).

An example of closed loop simulation for pulse #74104 is shown below. The outputs shown here are the plasma current, the position of the null point, the current in the in-vessel coils, the controlled flux differences and the shape of the plasma at $t = 7\,, 8$ and 9 s.

5. Controller Design

The linearized models discussed in the previous sections can also be exploited to design model-based plasma magnetic controllers by means of well-assessed methodologies from classical control theory. In particular, they have

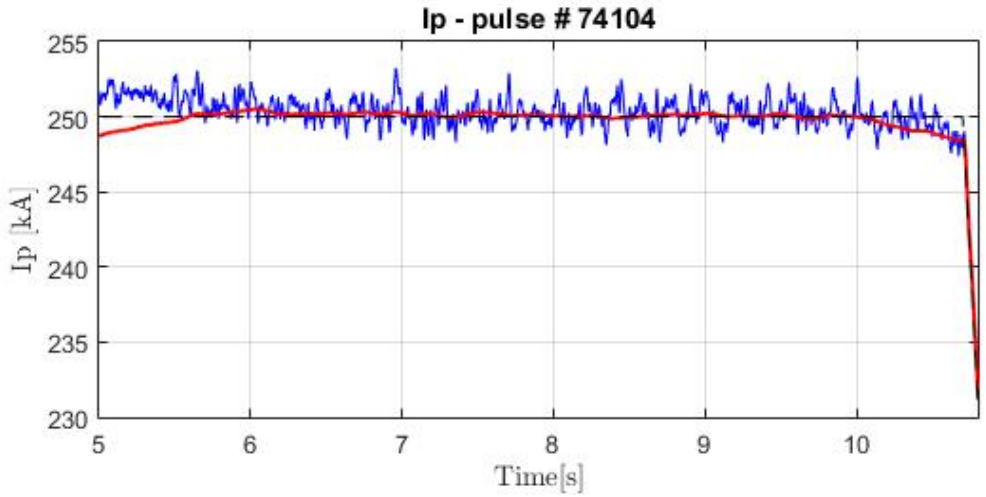

Figure 13: Simulated and experimental plasma current for pulse #74104. The experimental signal is shown in blue, while the simulated one is in red. The dashed black line shows the reference signal.

been used to design a new vertical stabilization system for the EAST tokamak, with voltage-driven in-vessel coils ([21], [22]) and an alternative position and plasma current controller ([23]), which have been successfully tested during the last experimental campaigns of EAST. Moreover, a multi-objective optimization of the VS system was performed in order to guarantee a good robustness over a wide range of plasma configurations ([24]).

Furthermore, a possible approach for an integrated control of plasma shape and flux expansion near the divertor plates has been proposed in [25]. Such an approach relies on a MIMO plasma shape controller, designed in a way which is similar to what has been done for the eXtreme Shape Controller (XSC) in JET ([26, 27]). It is worth to notice that, differently from what has been already done on the JET tokamak, the MIMO controller proposed for EAST adopts the isoflux logic, i.e. it controls poloidal flux differences instead of geometrical shape descriptors. This allows to test the new regulators with a minimum impact on the existing EAST PCS architecture. Controllers of this kind should be tested during the next EAST experimental campaign.

For these reasons, the tools have been enhanced in order to automatically generate the decoupling matrices for the MIMO shape control, starting from

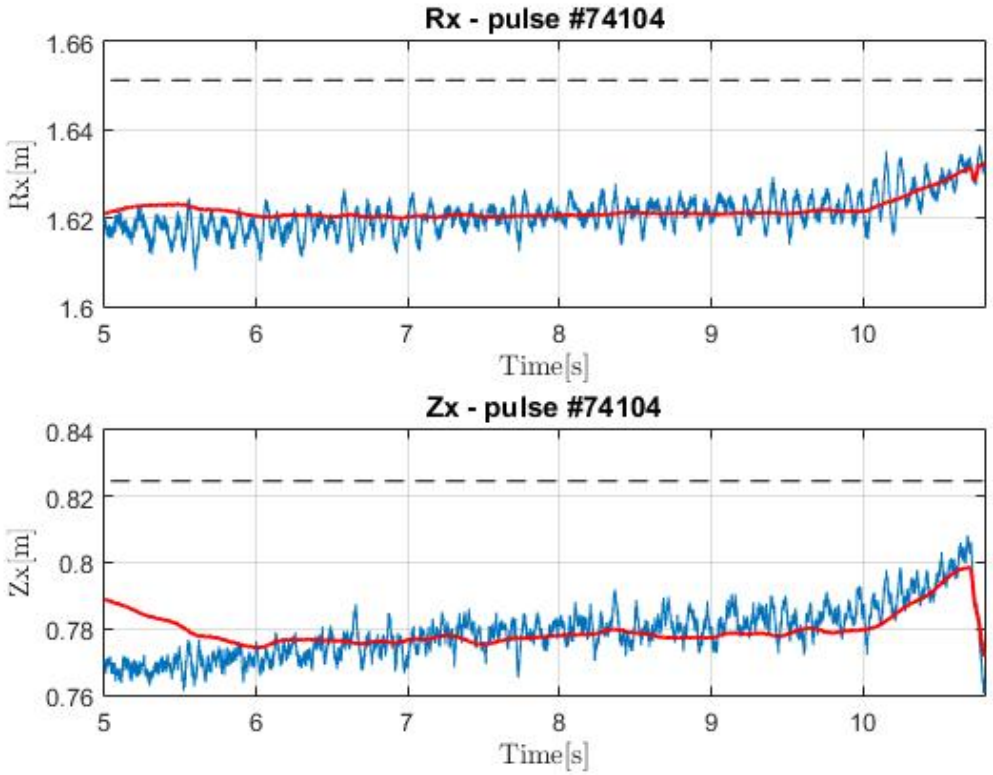

Figure 14: Simulated and experimental x-point position for pulse #74104. The experimental signal is shown in blue, while the simulated one is in red. The dashed black line shows the reference signal.

the static state-output relation of the linearized model. An example of MIMO control for EAST pulse #74104 is shown below. For the purposes of this simulation, the experimental traces of poloidal beta and internal inductance have been keept as inputs to the system, in order to test the disturbances rejection rate of the controller. The figures show a comparison between the actual shape controller installed on EAST and the simulated XSC controller for the same pulse.

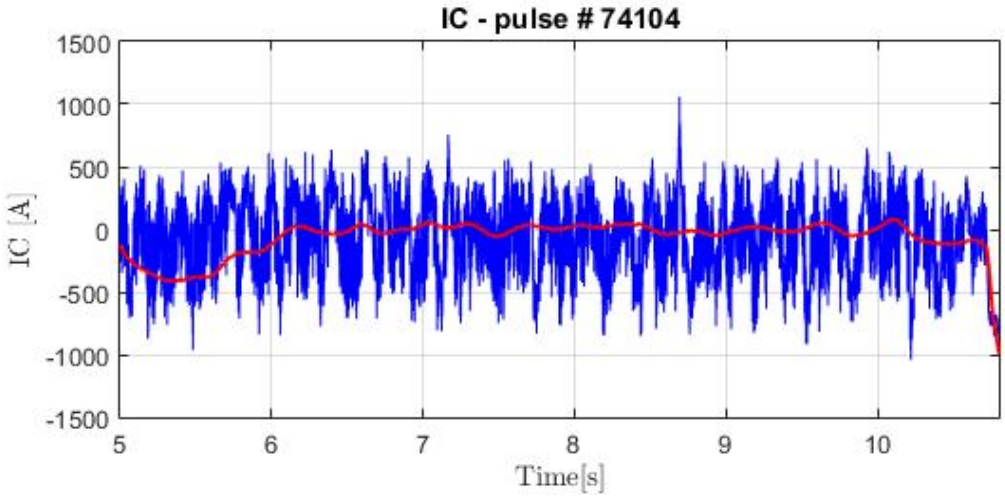

Figure 15: Simulated and experimental in-vessel circuit current for pulse #74104. The experimental signal is shown in blue, while the simulated one is in red.

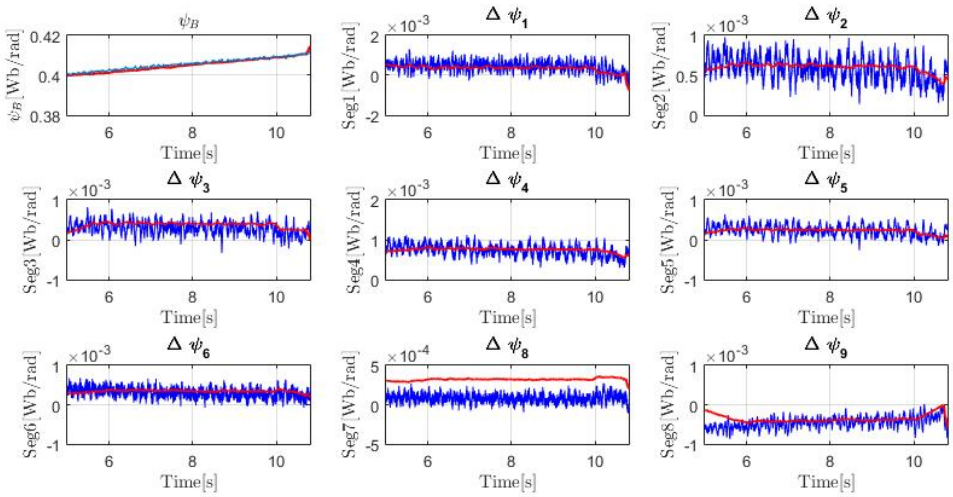

Figure 16: Simulated and experimental boundary flux and controlled flux differences for pulse #74104. The experimental signal is shown in blue, while the simulated one is in red.

6. Conclusions and Future work

In this paper, a simulation tools suite for the EAST tokamak was presented. These tools are based on a well-tested numerical code and allow the

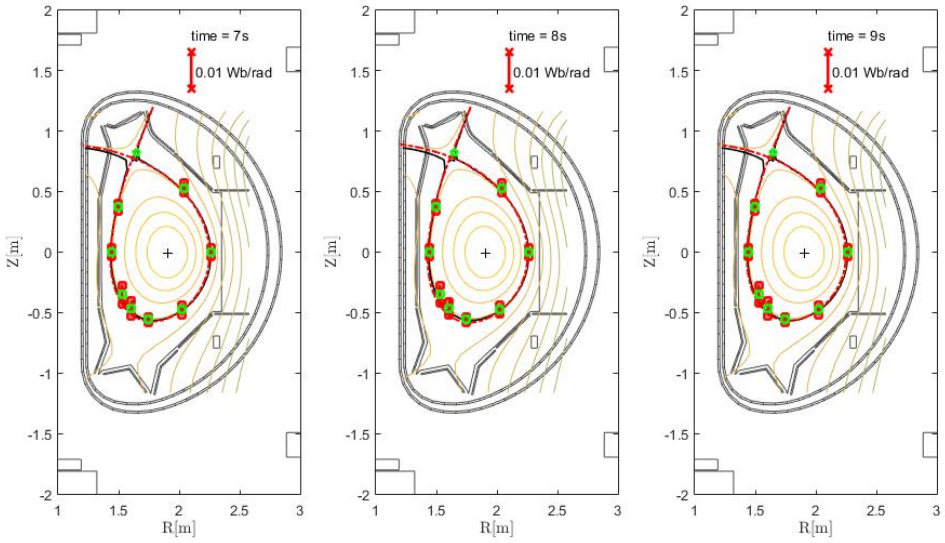

Figure 17: Reconstruction of flux map and plasma contour for pulse #74104 at 7, 8 and 9 s. The green markers represent the reference shape, while the red bars show the flux error at the control points. The experimental shape, reconstructed by EFIT, is shown by the red dashed line.

user to easily reproduce the EAST experiments. However, there is still much work to do, in order to further refine the simulator and well-reproduce in detail all the different magnetic configurations performed at EAST, such as double null and quasi-snowflake discharges. This would lead to an improved flexibility in the simulation environment, allowing to explore new control algorithms, i.e. for regulating the flux expansion near the divertor plates (see, for example, [25]). The tools presented here have been used for the design of a new Vertical Stabilization system and an alternative RZ controller, which have already been tested on the machine. MIMO shape control algorithms are being currently developed and should be tested in the next experimental campaigns.

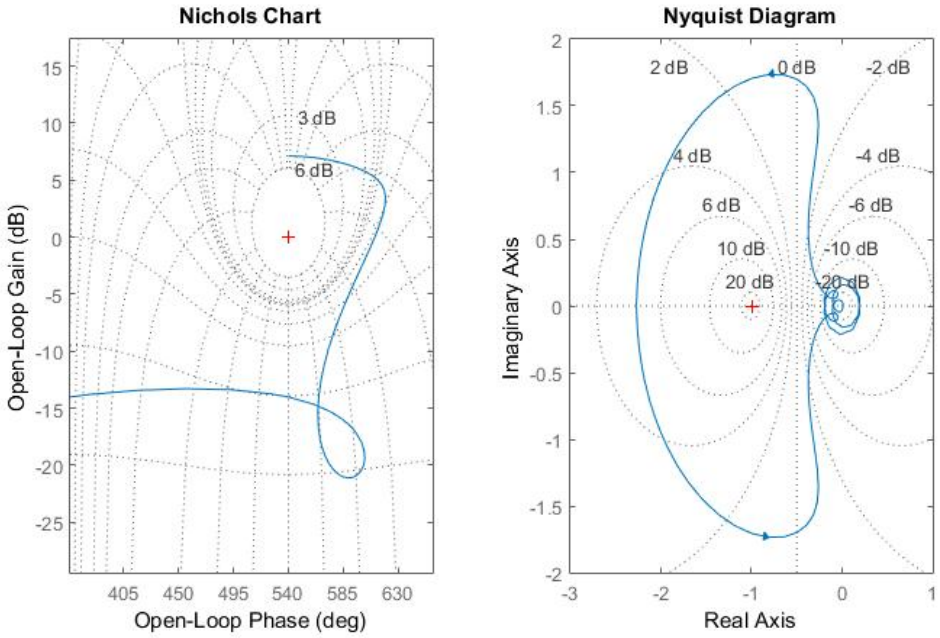

Figure 18: Nichols and Nyquist charts for the VS system for pulse #74104.

Acknowledgements

This work has been carried out within the framework of the EUROfusion Consortium and has received funding from the Euratom research and training programme 2014-2018 under grant agreement No 633053. The views and opinions expressed herein do not necessarily reflect those of the European Commission.

[1] G. Calabró, et. al., EAST Alternative Magnetic Configurations: Modelling and First Experiments, Nuclear Fusion 55 (2015) 1–11.

[2] G. Cenacchi, A. Taroni, JETTO: a free boundary plasma transport code, Technical Report 5, ENEA, Rome (Italy), 1988.

[3] G. Pereverzev, A. N. Yushmanov, ASTRA: automated system for transport analysis in a tokamak, Technical Report 5/98, Max-Planck-Institut fur Plasmaphysik, Garching bei Munich (Germany), 2002.

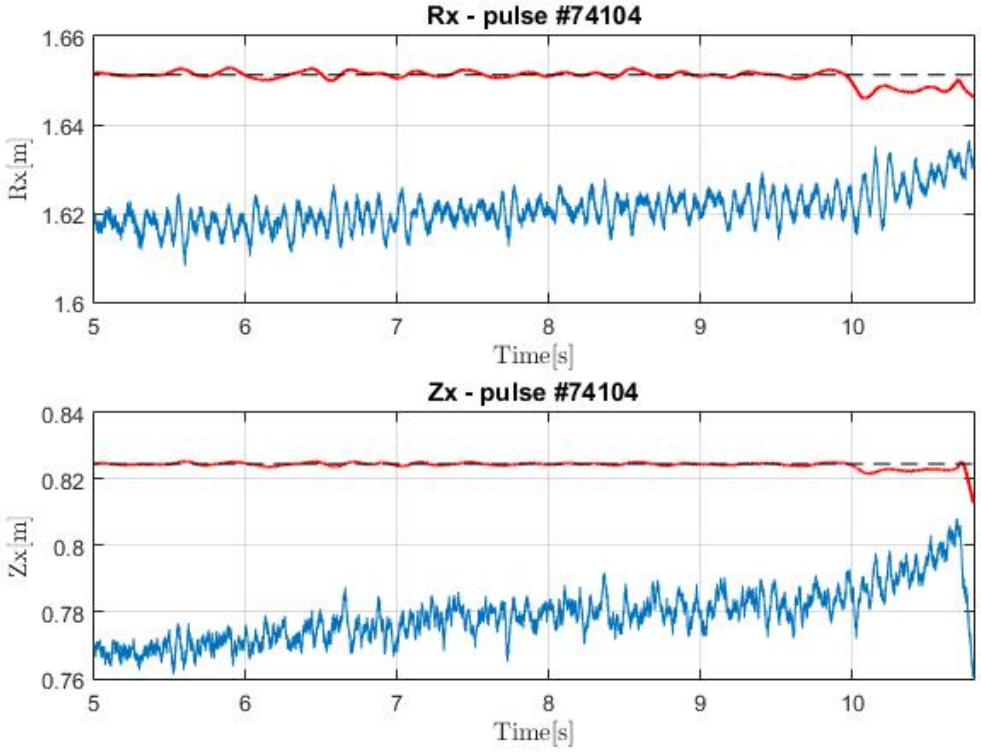

Figure 19: Simulated and experimental x-point position for pulse #74104. The experimental signal is shown in blue, while the simulated one is in red. The dashed black line shows the reference signal.

[4] J. Artaud, et al., The CRONOS suite of codes for integrated tokamak modelling, Nucl. Fus. 50 (2010) 043001.

[5] V. Parail, et al., Self-consistent simulation of plasma scenarios for ITER using a combination of 1.5D transport codes and free- boundary equilibrium codes, Nucl. Fus. 53 (2013) 113002.

[6] A. Coutlis, et al., Measurement of the open loop plasma equilibrium response in TCV, Nucl. Fus. 39 (1999) 663–683.

[7] D. Humphreys, et al., DIII-D Integrated plasma control solutions for ITER and next-generation tokamaks, Fus. Eng. Des. 83 (2008) 193–197.

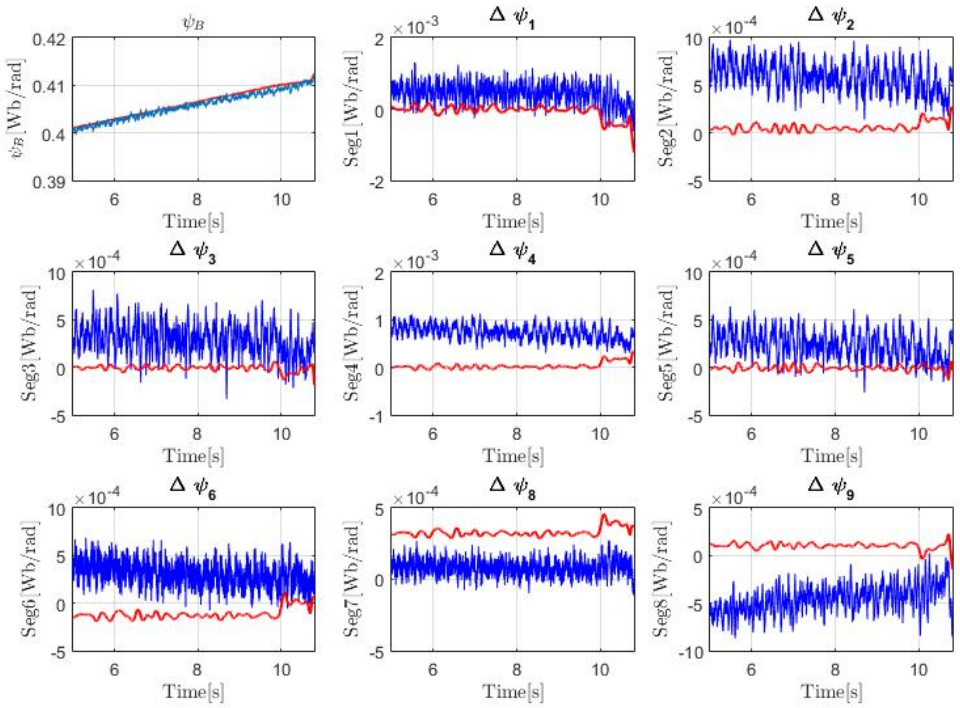

Figure 20: Simulated and experimental boundary flux and controlled flux differences for pulse #74104. The experimental signal is shown in blue, while the simulated one is in red.

[8] F. Felici, et al., Real-time physics-model-based simulation of the current density profile in tokamak plasmas, Nucl. Fus. 51 (2011) 083052.

[9] G. De Tommasi, et al., XSC Tools: a software suite for tokamak plasma shape control design and validation, IEEE Trans. Plasma Sci. 35 (2007) 709–723.

[10] F. Felici, et al., Development of real-time plasma analysis and control algorithms for the TCV tokamak using Simulink, Fus. Eng. Des. 89 (2014) 165–176.

[11] G. Marchiori, et al., Design and operation of the RFX-mod plasma shape control system, Fus. Eng. Des. 108 (2016) 81–91.

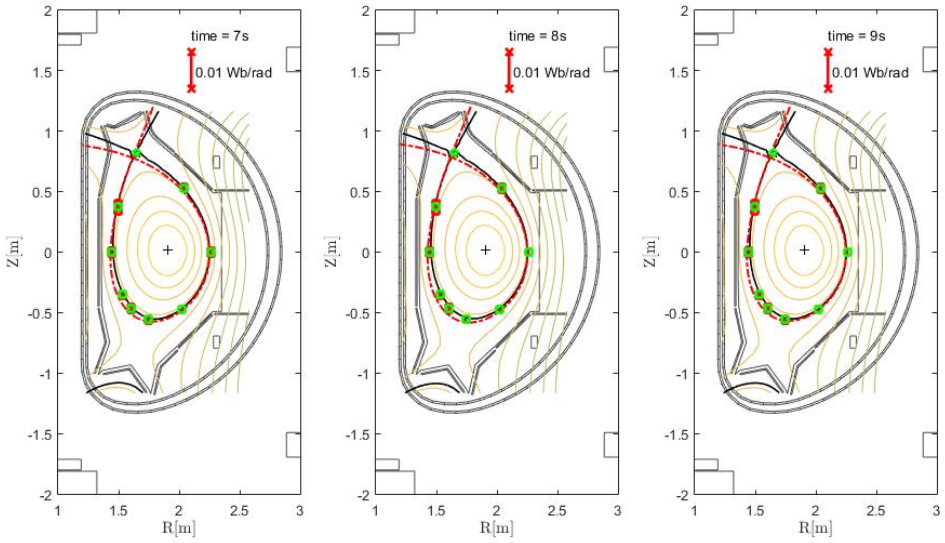

Figure 21: Reconstruction of flux map and plasma contour for pulse #74104 at 7, 8 and 9 s. The green markers represent the reference shape, while the red bars show the flux error at the control points. The experimental shape, reconstructed by EFIT, is shown by the red dashed line.

[12] S. Peruzzo, et al., Installation and commissioning of the JET-EP magnetic diagnostic system, Fus. Eng. Des. 84 (2009) 1495–1498.

[13] R. Albanese, R. Ambrosino, M. Mattei, CREATE-NL+: A robust control-oriented free boundary dynamic plasma equilibrium solver, Fus. Eng. Des. 96–97 (2015) 664–667.

[14] R. Albanese, F. Villone, The linearized CREATE-L plasma response model for the control of current, position and shape in tokamaks, Nuclear Fusion 38 (1998) 723–738.

[15] G. Manduchi, et al., MDSplus evolution continues, Fusion Engineering and Design 87 (2012) 2095–2099.

[16] L. Lao, H. S. John, R. Stambaugh, A. Kellman, W. Pfeiffer, Recon-

struction of current profile parameters and plasma shapes in tokamaks, Nuclear fusion 25 (1985) 1611.

[17] R. Albanese, G. Artaserse, F. Maviglia and F. Sartori, Identification of Vertical Instabilities in JET Tokamak, IEEE Trans. Magnetics 44 (2008) 1650–1653.

[18] J. Ferron, et al., Real time equilibrium reconstruction for tokamak discharge control, Nuclear Fusion 38 (1998) 1055.

[19] Y. Huang, et al., Implementation of GPU parallel equilibrium reconstruction for plasma control in EAST, Fus. Eng. Des. 112 (2016) 1019–1024.

[20] Q. P. Yuan and others, Plasma current, position and shape feedback control on EAST, Nuclear Fusion 53 (2013) 043009.

[21] R. Albanese, et al., ITER-like Vertical Stabilization System for the EAST tokamak, Nuclear Fusion 57 (2017).

[22] G. De Tommasi, et al., On plasma vertical stabilization at EAST tokamak, in: Proc. 2017 IEEE Conference on Control Technology and Applications (CCTA), Kohala Coast, Hawai'i, USA, pp. 511–516.

[23] B. Xiao, et al., Model Based plasma vertical stabilization and position control at EAST, in: 11th IAEA Technical Meeting on Control, Data Acquisition, and Remote Participation for Fusion Research, Greifswald, Germany.

[24] G. De Tommasi, A. Mele, A. Pironti, Robust plasma vertical stabilization in tokamak devices via multi-objective optimization, in: International Conference on Optimization and Decision Science, pp. 305–314.

[25] R. Albanese, et al., A MIMO architecture for integrated control of plasma shape and flux expansion for the EAST tokamak, in: Proc. of the 2016 IEEE Multi-Conference on Systems and Control, Buenos Aires, Argentina, pp. 611–616.

[26] M. Ariola, A. Pironti, The design of the eXtreme Shape Controller for the JET tokamak, IEEE Control Sys. Mag. 25 (2005) 65–75.

[27] R. Albanese, et al., Design, implementation and test of the XSC extreme shape controller in JET, Fus. Eng. Design 74 (2005) 627–632.